The Nature of Chemisorbed CO_2 in Zeolite A

Przemyslaw Rzepka[a], Zoltán Bacsik[a], Andrew J. Pell[a], Niklas Hedin[a,*], and Aleksander Jaworski[a,*]

[a]Department of Materials and Environmental Chemistry, Stockholm University, SE-106 91 Stockholm, Sweden

*Corresponding authors: *aleksander.jaworski@mmk.su.se*, *niklas.hedin@mmk.su.se*

Abstract

Formation of CO_3^{2-} and HCO_3^- species without participation of the framework oxygen atoms upon chemisorption of CO_2 in zeolite $|Na_{12}|$-A is revealed. The transfer of O and H atoms is very likely to have proceeded via the involvement of residual H_2O or $-OH$ groups. A combined study by solid-state ^1H and ^{13}C MAS NMR, quantum chemical calculations, and *in situ* IR spectroscopy showed that the chemisorption mainly occurred by the formation of HCO_3^-. However, at a low surface coverage of physisorbed and acidic CO_2, a significant fraction of the HCO_3^- was deprotonated and transformed into CO_3^{2-}. We expect that similar chemisorption of CO_2 would occur for low-silica zeolites and other basic silicates of interest for the capture of CO_2 from gas mixtures.

TOC Graphic

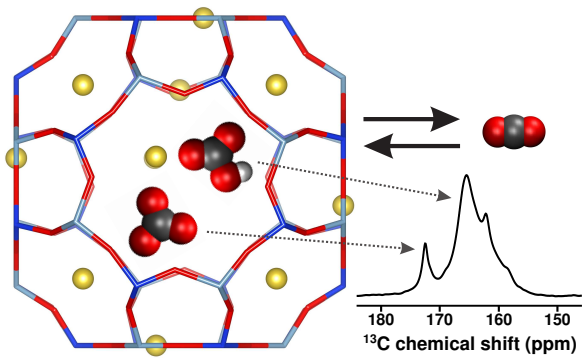

Keywords: Zeolites, Chemisorption, CO_2 capture and storage (CCS), Adsorption, Bicarbonates, Carbonates, NMR, DFT

Adsorption-driven separation of CO_2 from flue gas[1–3] and raw biogas[4,5] are of considerable interest for anthropogenic reasons. In relation to these processes, adsorbents such as zeolites, activated carbons, porous polymers, and amine-modified silica materials are being extensively studied.[1,2,6] It is generally found that CO_2 typically adsorbs by weak intermolecular interactions (physisorption),[7] but on sorbents of sufficiently high base strength chemisorption also occurs, especially when catalytic amounts of water are present.[8–12] For example, on low-silica zeolites with monovalent cations, CO_2 is both physisorbed and chemisorbed.[13–17] In contrast to physisorption, chemisorption results in the molecular structure of CO_2 being significantly altered. However, to date the mechanisms of chemisorption of CO_2 on zeolites, and the nature of the species formed, are not well understood. This was the problem we undertook to address in this study, and we were able to identify the species formed on chemisorption of CO_2 by using a combination of ^{1}H and ^{13}C solid-state nuclear magnetic resonance (NMR), density-functional theory (DFT), and *in situ* infrared (IR) spectroscopy.

The physisorption of CO_2 on zeolites[15,18–20] is mainly due to the interaction between the relatively large molecular electric quadrupole moment of CO_2, and the significant electric field gradients near the zeolite framework. In parallel, low-silica zeolites such as zeolite X,[19,21–23] Y,[14,23,24] and A[19,22] also chemisorb CO_2 resulting in the formation of $(H)CO_3^{(-)2-}$ species. Even though the positioning of the chemisorbed species at the 8-ring of zeolite A was partially determined by Rzepka *et al.*,[25] with *in situ* neutron diffraction (ND), the precise chemical nature of these $(H)CO_3^{(-)2-}$ species has hitherto remained unknown. It has been speculated that either CO_2 reacts with the O-atoms of the framework[21–24] forming framework-linked species,[14,19,22,24] or that residual H_2O or $-OH$ groups are involved in forming $(H)CO_3^{(-)2-}$ species.[13,14,24]

The fraction of CO_2 chemisorbed by the system in this study, zeolite $|Na_{12}|$-A, was assessed indirectly by volumetric adsorption measurements[17,26] of the first two adsorption-desorption cy-

cles, as shown in Figure 1. A reduction in adsorption capacity during the second cycle relative to the first was observed, which was ascribed to the fraction of CO_2 that had been irreversibly chemisorbed, since the large majority of chemisorbed species cannot be removed by evacuation under high dynamic vacuum. A long evacuation was used to remove fractionally entrapped CO_2 before the second cycle,[27–29] and it was found that approximately 6% of the adsorbed CO_2 on zeolite $|Na_{12}|$-A was chemisorbed, corresponding to about 0.5 molecules per α-cage.

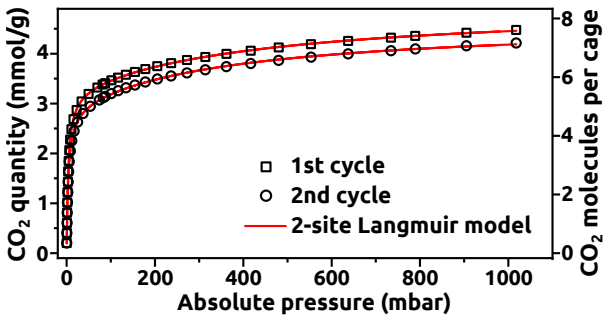

Figure 1. The quantity of adsorbed CO_2 vs pressure on zeolite $|Na_{12}|$-A at 293 K for a pristine sample (1st cycle) and after 12 h of re-evacuation under high dynamic vacuum (2nd cycle). The data conform to the two-site Langmuir model.

To identify the chemisorbed species, their quantities, and to gain insight into their dynamics, we employed ^{13}C solid-state magic-angle spinning (MAS) NMR spectroscopy. This technique has been recently and successfully used to investigate the details of chemisorbed CO_2 in amine-modified clays[9] and silicas,[10] metal organic frameworks,[11,30] polymers,[31] and layered hydroxides.[32] However, ^{13}C MAS NMR spectroscopy has to date not been used to study the chemisorption of CO_2 on zeolites. We employed a direct excitation (Bloch-decay) NMR protocol with 99% ^{13}C-enriched CO_2 to ensure a full visibility of the adsorbed species and quantitative character of the collected data.

The ^{13}C NMR spectrum at 5 kHz MAS of zeolite $|Na_{12}|$-A with 1 bar of CO_2 is shown in Figure 2(e). Resonances with chemical shifts characteristic of both physisorbed and chemisorbed CO_2 were detected. The signals with isotropic shifts at 125 and 162 ppm correspond to physisorbed

CO_2,[33,34] and HCO_3^-, respectively. The H-transfer was likely to have occurred with the involvement

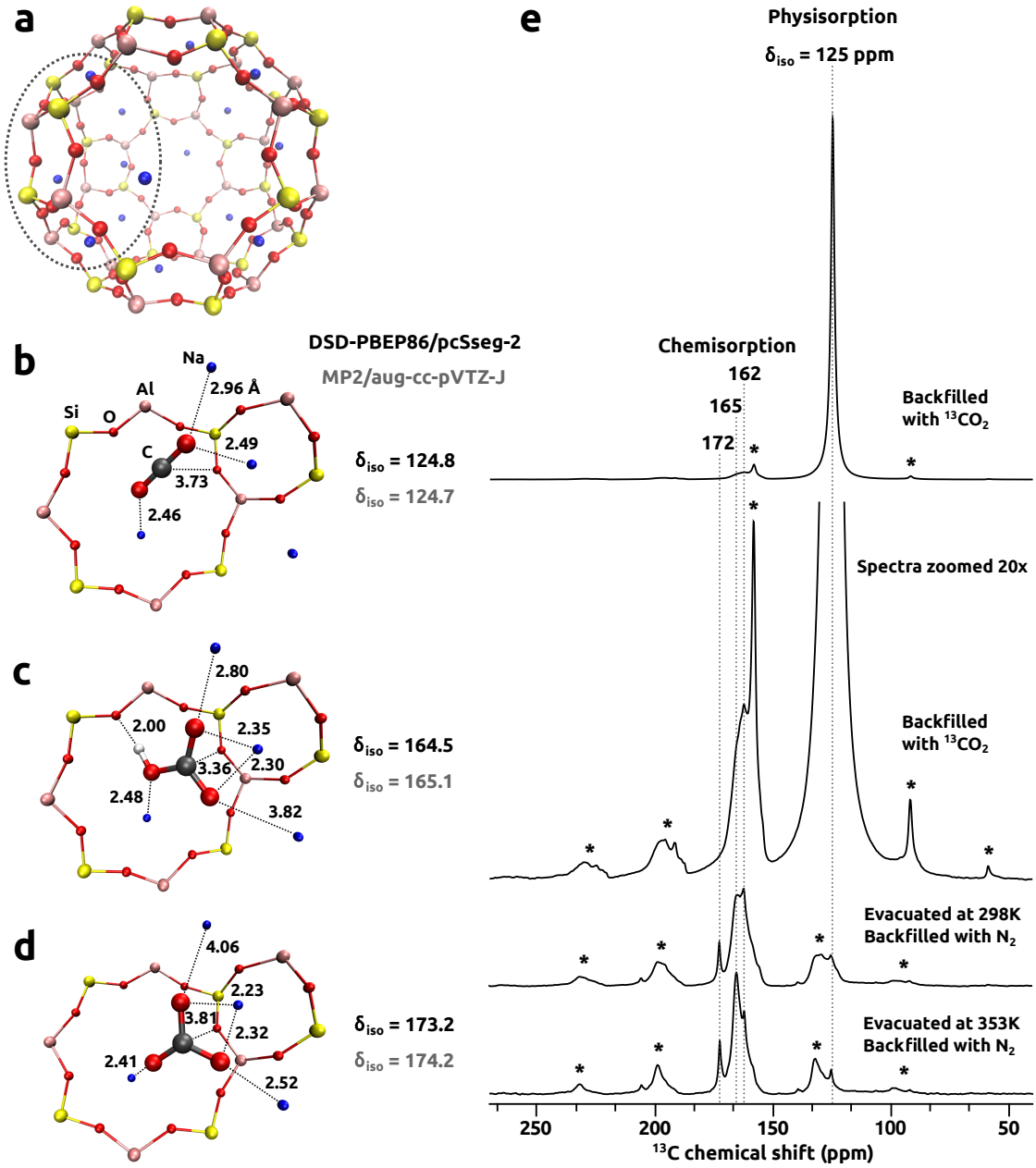

Figure 2. The α-cavity of zeolite $|Na_{12}|$-A (a); fragments of the models of CO_2 (b), HCO_3^- (c), and CO_3^{2-} (d) species inside the α-cavity resulting from geometry optimization at the OLYP-D3(BJ)/cc-pVTZ level of theory. ^{13}C isotropic chemical shifts calculated with GIAO method at the DSD-PBEP86/pcSseg-2 (black) and MP2/aug-cc-pVTZ-J (grey) level of theory. (e) ^{13}C MAS NMR spectra of CO_2 adsorbed in zeolite $|Na_{12}|$-A collected at 14.1 T and 5 kHz MAS rate. The spinning sidebands are marked with asterisks.

of H_2O or $-OH$ groups.[35] No CO_3^{2-} was observed under these conditions. The fraction of chemisorbed species as determined from integrating the ^{13}C MAS NMR resonances was 0.06 at

1 bar of CO_2, which is in an excellent agreement with the fraction estimated from the volumetric adsorption data.

The bottom two solid-state ^{13}C MAS NMR spectra of Figure 2(e) were collected from zeolite $|Na_{12}|$-A following saturation with 1 bar of CO_2, subjected to evacuation under high dynamic vacuum for 12 h at the respective temperatures of 298 and 353 K, and backfilled with 1 bar of N_2. In both these cases, the intensity of the signal with isotropic shift of 125 ppm was reduced substantially, indicating that very little physisorbed CO_2 remained, and the resonances at 162−172 ppm originate exclusively from chemisorbed species. The signals with isotropic shifts at 165 and 162 ppm were hypothesized to correspond to two different types of HCO_3^-, whereas that at 172 ppm was attributed to CO_3^{2-}. Similar assignments were reported by Ishihara *et al.* for the adsorption of CO_2 on hydrotalcite. The relative fraction of the CO_3^{2-}, to the full amount of chemisorbed CO_2, was 0.06 for the system evacuated at 298 K, and 0.11 for that evacuated at 353 K. The increased relative fraction of CO_3^{2-} was consistent with a heat- and vacuum-enhanced desorption of CO_2 or H_2O, and in line with the *in situ* IR spectroscopy observations. Concurrently with the elevated desorption temperature of CO_2, there were alterations towards higher populations of both carbonates (172 ppm), and bicarbonate species with a shift of 165 ppm, at the expense of the bicarbonate species with an isotropic shift of 162 ppm.

To corroborate the NMR assignments and derive molecular representations for the adsorption of CO_2, we calculated the ^{13}C NMR chemical shifts on DFT-derived models. The corresponding molecular representations and calculated chemical shifts are presented in Figure 2(b−d). The energy-optimized positions of the CO_2, HCO_3^-, and CO_3^{2-} were in accordance to those refined from ND data by Rzepka *et al.* At the dispersion-corrected OLYP-D3(BJ)/cc-pVTZ level of theory[36–41] employed in the optimization of the DFT models, the potential energy surface did not reveal an energy minimum corresponding to the CO_2 molecule binding with framework −O− bridge for any of

the several starting configurations used. The calculations indicate that the distance between the C atom of HCO_3^- and the framework O atom is 3.36 Å (Figure 2(c)), which is in a good agreement with the value of 3.3 Å from the previous ND refinement of the chemisorbed CO_2 positions performed for the same system.[25] At this distance, we could infer that there is no participation of the framework O-atom in covalent bonding with a HCO_3^- moiety. The same conclusion can be reached for the CO_3^{2-} group (Figure 2(d)), where the C is 3.81 Å from the framework O. Hence, we concluded that both the HCO_3^- and CO_3^{2-} form as self-standing entities in the zeolite α-cavity without any participation of framework $-$O$-$ bridge. For ^{13}C chemical shifts assignments the GIAO approach with the perturbatively-corrected, double-hybrid DFT (DHDFT) DSD-PBEP86 approximation, as well as the second-order Møller-Plesset perturbation theory (MP2) were employed.[42–44] These are currently the most accurate (affordable) methods for NMR shielding tensors calculations, when combined with NMR-optimized basis sets: pcSseg-n and aug-cc-pVTZ-J.[45–48] We observed that the chemical shifts calculated on our models at both DHDFT and MP2 level of theory were in excellent agreement with those measured experimentally. In particular, we note that the shifts in Figure 2(c,d) of 164.5$-$165.1 and 173.2$-$174.2 ppm were due to HCO_3^- and CO_3^{2-} ions, respectively, and not to physisorbed CO_2, which gave a lower shift of 124.7$-$124.8 ppm (Figure 2(b)).

To provide experimental evidence for bicarbonate formation upon chemisorption of CO_2 on zeolite |Na_{12}|-A, fast-MAS ^{1}H and ^{1}H$\rightarrow^{13}$C cross-polarization (CP) MAS NMR experiments were performed. Here we note that traditional CPMAS approaches have very recently been shown to be problematic in studies of HCO_3^- chemisorbed onto amine-modified mesoporous silica sorbents.[12] In Figure 3(a), high-resolution (60 kHz MAS) ^{1}H NMR spectra of activated zeolite |Na_{12}|-A (dried under high dynamic vacuum at 623 K for 24 h), as well as the zeolite containing chemisorbed CO_2 are presented. The activated zeolite contained non-negligible amounts of H_2O and $-$OH groups, as was indicated by several overlapping ^{1}H resonances in the 0$-$8 ppm range. Upon chemisorption

of CO_2 signals at 12 and 16 ppm emerge at the expense of those from −OH groups and residual H_2O. These resonances were assigned to bicarbonate species, as their chemical shifts are in good

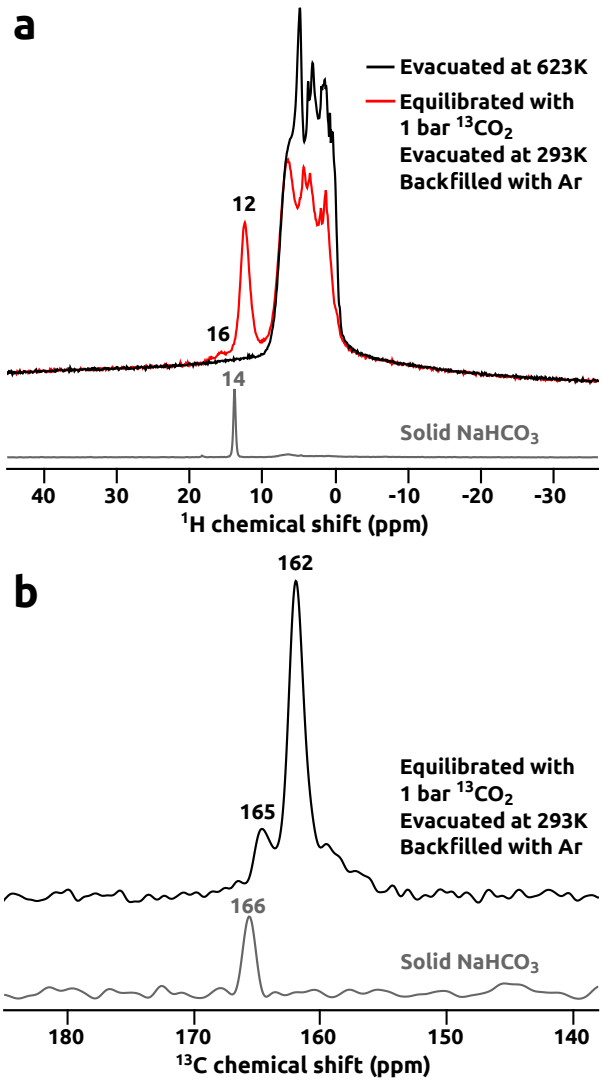

Figure 3. (a) ^{1}H MAS NMR spectra of activated zeolite |Na_{12}|-A (black), zeolite |Na_{12}|-A equilibrated with 1 bar of $^{13}CO_2$ and backfilled with Ar (red), shown together that of solid $NaHCO_3$ (grey). The data collected at 14.1 T and 60 kHz MAS rate. (b) ^{1}H→^{13}C CPMAS spectrum of zeolite |Na_{12}|-A equilibrated with 1 bar of $^{13}CO_2$ and backfilled with Ar (black), and that of solid $NaHCO_3$ (grey); both spectra acquired at 14.1 T and 14 kHz MAS rate.

agreement with the shift of 14 ppm from pure, solid $NaHCO_3$. Furthermore, the formation of bicarbonate was unambiguously evidenced by ^{1}H→^{13}C CPMAS spectra in Figure 3(b). ^{13}C chemical shifts of 162 and 165 ppm were close to that of 166 ppm from solid $NaHCO_3$, and same as

directly-excited counterparts in Fig. 2(e), indicating two distinct bicarbonate environments, in line with ^{1}H spectrum in Fig. 3(a). Note that in the directly-excited ^{13}C MAS NMR spectra of the evacuated samples (Fig. 2(e); bottom traces) signal with isotropic shift of 172 ppm was observed. The absence of this resonance in ^{1}H$\rightarrow^{13}$C CPMAS spectrum corroborates the assignment to CO_3^{2-}.

We also studied the chemisorption of CO_2 in zeolite $|Na_{12}|$-A with *in situ* IR spectroscopy. For zeolites with relatively high basicity, IR spectral features of chemisorbed CO_2 are usually observed by C$-$O stretching bands in the range of 1800$-$1200 cm^{-1}, and typically assigned to carbonate-like species.[13,14,24,49,50] However, the bands in this spectral region are quite complex and not always straightforward to interpret. The symmetrical (free) carbonate ion has a single band around 1415 cm^{-1}, but upon lowering the symmetry, this double degenerated vibration splits into two distinct IR bands for the asymmetric stretching mode. The extent of this split has been used for identification of chemisorbed species,[51] and for zeolite 4A these band pairs have been assigned to monodentate, bidentate, and chelating coordinated carbonate species.[49] Although our IR spectra shown in Figure 4 are very similar to those reported by Montanari *et al.*, the presence of bicarbonate cannot be excluded, because of the same nature of bands split for asymmetric C$-$O stretches of bicarbonate and these carbonate species. The band pair at 1726 and 1250 cm^{-1} originate from labile carbonate or bent CO_2 species that are present only at higher CO_2 pressures. The overlapping band pairs around 1624 and 1365 cm^{-1} can either be assigned to bidentate carbonate species or to HCO_3^-. The bicarbonate formation is suggested by a broad H-bonded $-$OH group band around 3250 cm^{-1} at low partial pressures of CO_2 (Figure 4(b)) that appear in parallel with the C$-$O bands at 1600 and 1385 cm^{-1}. Moreover, a negative intensities are observed in the $-$OH stretching region around 3635 cm^{-1}, which compares well with 3608 cm^{-1} reported for residual $-$OH groups in activated zeolite A by Montanari *et al.* This may indicate that $-$OH groups are "consumed" and the new band result from $-$OH vibrations in bicarbonate moiety. This effect is enhanced in

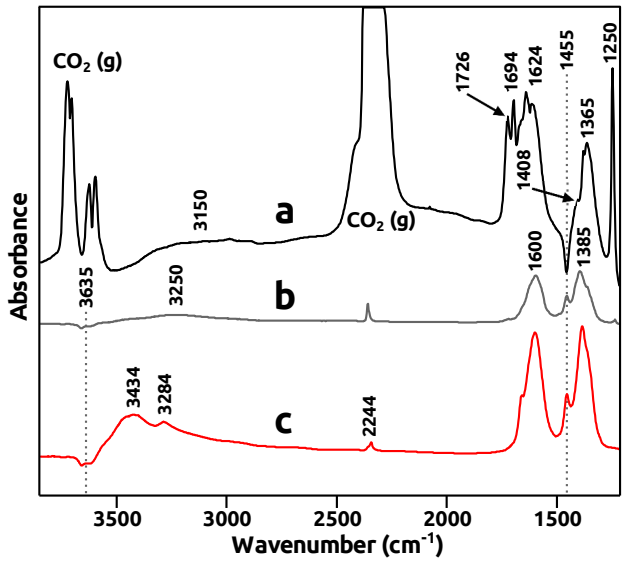

Figure 4. *In situ* IR spectra of zeolite |Na_{12}|-A: under 1 bar of CO_2 (a), 0.00003 bar of CO_2 (b), and after evacuation under high dynamic vacuum for 4 h (c).

the spectrum of evacuated zeolite, where negative intensities around 3635 cm^{-1} are accompanied by two distinct bands of H-bonded −OH groups at 3434 and 3284 cm^{-1} (Figure 4(c)). The appearance of these two bands is in agreement with ^{1}H MAS NMR spectra of Figure 3(a). At low CO_2 pressure, and after evacuation (Figure 4(b,c)), there is a single band of the antisymmetric stretching mode at 1455 cm^{-1} observed, which we attribute to symmetrical and planar CO_3^{2-}, but we cannot exclude that it might be a high frequency component of the band pair with its lower frequency counterpart appearing as a shoulder on the band at 1385 cm^{-1}. Note that the intensity ratios of these carbonates are not fully correct in the spectra of Fig. 4(b,c) since these species are already present in activated zeolite as indicated by the negative band at 1455 cm^{-1} in Fig. 4(a). The transformations of different carbonate-like species upon CO_2 pressure/coverage changes *i.e.* symmetric carbonates at low, and less symmetric species at high have also been observed by others on zeolite A[49] and zeolite X.[13]

To conclude, it is established that the chemisorption of CO_2 in low-silica zeolites involves basic sites (conjugate acid-base pairs).[52–55] However, in this study we showed for the first time that carbonates did not integrate with the framework of zeolite |Na_{12}|-A. We also showed that two

different types of HCO_3^- formed and that CO_3^{2-} occurred at very small pressures of CO_2. As the formation of CO_3^{2-} is favored only in highly basic environment,[12] it was consistent that CO_3^{2-} was stabilized at low concentrations of CO_2 on the zeolite $|Na_{12}|$-A. We expect that similar equilibria among different coexisting chemisorbed species and their dependencies on the temperature and overall CO_2 surface coverage to be observed for other zeolites and basic (alumino)silicates in general.

Acknowledgements

The research was financially supported by the Swedish Research Council (VR), grant numbers: 2016-03441 (AJP and AJ) and 2016-03568 (NH, PR, and ZB).

Supporting Information Available: methodology of NMR experiments, quantum chemical calculations, volumetric adsorption measurements, *in situ* IR spectroscopy, parameters of the two-site Langmuir model, ^{1}H MAS NMR spectrum of zeolite $|Na_{12}|$-A exposed to moisture.

References

[1] Choi, S.; Drese, J. H.; Jones, C. W. Adsorbent Materials for Carbon Dioxide Capture from Large Anthropogenic Point Sources. *ChemSusChem* **2009**, *2* (9), 796–854.

[2] D'Alessandro, D. M.; Smit, B.; Long, J. R. Carbon Dioxide Capture: Prospects for New Materials. *Angew. Chem.* **2010**, *49* (35), 6058–6082.

[3] Webley, P. A. Adsorption Technology for CO_2 Separation and Capture: A Perspective. *Adsorption* **2014**, *20* (2-3), 225–231.

[4] Wang, D.; Zhao, T.; Cao, Y.; Yao, S.; Li, G.; Huo, Q.; Liu, Y. High Performance Gas Adsorption and Separation of Natural Gas in Two Microporous Metal-Organic Frameworks with Ternary Building Units. *Chem. Commun.* **2014**, *50* (63), 8648–8650.

[5] Sun, Q.; Li, H.; Yan, J.; Liu, L.; Yu, Z.; Yu, X. Selection of Appropriate Biogas Upgrading Technology−A Review of Biogas Cleaning, Upgrading and Utilisation. *Renew. Sustain. Energy Rev.* **2015**, *51*, 521–532.

[6] Moliner, M.; Martínez, C.; Corma, A. Synthesis Strategies for Preparing Useful Small Pore Zeolites and Zeotypes for Gas Separations and Catalysis. *Chem. Mater.* **2014**, *26* (1), 246–258.

[7] Oura, K.; Katayama, M; Zotov, A.; Lifshits, V; Saranin, A. A., *Surface Science: An Introduction*, Springer, Berlin **2003**.

[8] Demessence, A; D'Alessandro, D. M.; Foo, M. L.; Long, J. R. Strong CO_2 Binding in a Water-Stable, Triazolate-Bridged Metal-Organic Framework Functionalized with Ethylenediamine. *J. Am. Chem. Soc.* **2009**, *131* (25), 8784–8786.

[9] Pinto, M. L.; Mafra, L.; Guil, J. M.; Pires, J.; Rocha, J. Adsorption and Activation of CO_2 by

Amine-Modified Nanoporous Materials Studied by Solid-State NMR and $^{13}CO_2$ adsorption. *Chem. Mater.* **2011**, *23* (6), 1387–1395.

[10] Mafra, L.; Čendak, T.; Schneider, S.; Wiper, P. V.; Pires, J.; Gomes, J. R. B.; Pinto, M. L. Structure of Chemisorbed CO_2 Species in Amine-Functionalized Mesoporous Silicas Studied by Solid-State NMR and Computer Modeling. *J. Am. Chem. Soc.* **2017**, *139* (1), 389–408.

[11] Milner, P. J.; Siegelman, R. L.; Forse, A. C.; Gonzalez, M. I.; Runčevski, T.; Martell, J. D.; Reimer, J. A.; Long, J. R. A Diaminopropane-Appended Metal-Organic Framework Enabling Efficient CO_2 Capture from Coal Flue Gas via a Mixed Adsorption Mechanism. *J. Am. Chem. Soc.* **2017**, *139* (38), 13541–13553.

[12] Chen, C. H.; Shimon, D.; Lee, J. J.; Mentink-Vigier, F.; Hung, I.; Sievers, C.; Jones, C. W.; Hayes, S. E. The "Missing" Bicarbonate in CO_2 Chemisorption Reactions on Solid Amine Sorbents. *J. Am. Chem. Soc.* **2018**, *140* (28), 8648–8651.

[13] Bertsch, L.; Habgood, H. W. An Infrared Spectroscopic Study of the Adsorption of Water and Carbon Dioxide by Linde Molecular Sieve X. *J. Phys. Chem.* **1963**, *67* (8), 1621–1628.

[14] Jacobs, P. A.; Van Cauwelaert, F. H.; Vansant, E. F.; Uytterhoeven, J. B. Surface Probing of Synthetic Faujasites by Adsorption of Carbon Dioxide. Part 1.−Infrared Study of Carbon Dioxide Adsorbed on Na-Ca-Y and Na-Mg-Y Zeolites. *J. Chem. Soc. Faraday Trans.* **1973**, *69* (1), 1056–1068.

[15] Delaval, Y.; de Lara, E. C. Study of Physisorption of Carbon Dioxide on NaA Zeolite. Part 1.−Experimental Results Obtained by Infrared Spectroscopy. *J. Chem. Soc. Faraday Trans.* **1981**, *77* (4), 869–877.

[16] Förster, H.; Schumann, M. Infrared Spectroscopic Studies on Carbon Dioxide Adsorption

in Alkali-Metal and Alkaline-Earth-Metal Ion-Exchanged A-Type Zeolites. Part 1.−General Features of CO_2 interaction with A-Type Zeolites. *J. Chem. Soc. Faraday Trans.* **1989**, *85* (5), 1149–1158.

[17] Rzepka, P.; Wardecki, D.; Smeets, S.; Müller, M.; Gies, H.; Zou, X.; Hedin, N. CO_2-Induced Displacement of $Na^+$and K^+ in Zeolite |NaK|-A. *J. Phys. Chem. C* **2018**, *122* (30), 17211–17220.

[18] Delaval, Y.; de Lara, E. C. Study of Physisorption of Carbon Dioxide on NaA Zeolite. Part 2.−Interpretation of Infrared Spectra from Statistical Models.. *J. Chem. Soc. Faraday Trans.* **1981**, *77* (4), 879–888.

[19] Amari, D.; Lopez Cuesta, J. M.; Nguyen, N. P.; Jerrentrup, R.; Ginoux, J. L. Chemisorption and Physisorption of CO_2 on Cation Exchanged Zeolites A, X and MOR. *J. Therm. Anal.* **1992**, *38* (4), 1005–1015.

[20] Yang, R. T., *Adsorbents : Fundamentals and Applications*, Wiley, New Jersey **2003**.

[21] Jacobs, P. A.; Van Cauwelaert, F. H.; Vansant, E. F.; Uytterhoeven, J. B. Surface Probing of Synthetic Faujasites by Adsorption of Carbon Dioxide. Part 2.−Infrared Study of Carbon Dioxide Adsorbed on X Zeolites Exchanged with Mono- and Bi-Valent Ions. *J. Chem. Soc. Faraday Trans.* **1973**, *69* (1), 2130–2139.

[22] Siriwardane, R. V.; Shen, M.-S.; Fisher, E. P.; Losch, J. Adsorption of CO_2 on Zeolites at Moderate Temperatures. *Energy & Fuels* **2005**, *19* (3), 1153–1159.

[23] Bonenfant, D.; Kharoune, M.; Niquette, P.; Mimeault, M.; Hausler, R. Advances in Principal Factors Influencing Carbon Dioxide Adsorption on Zeolites. *Sci. Technol. Adv. Mater.* **2008**, *9* (1), 1–7.

[24] Gallei, E.; Stumpf, G. Infrared Spectroscopic Studies of the Adsorption of Carbon Dioxide and the Coadsorption of Carbon Dioxide and Water on CaY- and NiY-Zeolites. *J. Colloid Interface Sci.* **1976**, *55* (2), 415–420.

[25] Rzepka, P.; Bacsik, Z.; Smeets, S.; Hansen, T. C.; Hedin, N.; Wardecki, D. Site-Specific Adsorption of CO_2 in Zeolite NaK-A. *J. Phys. Chem. C* **2018**, *122* (47), 27005–27015.

[26] Cheung, O.; Bacsik, Z.; Liu, Q.; Mace, A.; Hedin, N. Adsorption Kinetics for CO_2 on Highly Selective Zeolites NaKA and Nano-NaKA. *Appl. Energy* **2013**, *112* (510), 1326–1336.

[27] Karger, J.; Ruthven, D. M. On the Comparison Between Macroscopic and NMR Measurements of Intracrystalline Diffusion in Zeolites. *Zeolites* **1989**, *9* (4), 267–281.

[28] Krishna, R.; Van Baten, J. M. A Molecular Dynamics Investigation of the Diffusion Characteristics of Cavity-type Zeolites with 8-ring Windows. *Microporous Mesoporous Mater.* **2011**, *137* (1-3), 83–91.

[29] Bleken, B. T. L.; Lillerud, K. P.; Splith, T.; Pusch, A. K.; Stallmach, F. PFG NMR Diffusion Measurements of CH_4 and CO_2 Through Large ZSM-58-Crystals. *Microporous Mesoporous Mater.* **2013**, *182*, 25–31.

[30] Flaig, R. W.; Osborn Popp, T. M.; Fracaroli, A. M.; Kapustin, E. A.; Kalmutzki, M. J.; Altamimi, R. M.; Fathieh, F.; Reimer, J. A.; Yaghi, O. M. The Chemistry of CO_2 Capture in an Amine-Functionalized Metal-Organic Framework under Dry and Humid Conditions. *J. Am. Chem. Soc.* **2017**, *139* (35), 12125–12128.

[31] Moore, J. K.; Sakwa-Novak, M. A.; Chaikittisilp, W.; Mehta, A. K.; Conradi, M. S.; Jones, C. W.; Hayes, S. E. Characterization of a Mixture of CO_2 Adsorption Products in Hyperbranched Aminosilica Adsorbents by ^{13}C Solid-State NMR. *Environ. Sci. Technol.* **2015**, *49*

(22), 13684–13691.

[32] Ishihara, S.; Sahoo, P.; Deguchi, K.; Ohki, S.; Tansho, M.; Shimizu, T.; Labuta, J.; Hill, J. P.; Ariga, K.; Watanabe, K.; Yamauchi, Y.; Suehara, S.; Iyi, N. Dynamic Breathing of CO_2 by Hydrotalcite. *J. Am. Chem. Soc.* **2013**, *135* (48), 18040–18043.

[33] Stejskal, E. O.; Schaefer, Jacob; Henis, J. M.S.; Tripodi, M. K. Magic-Angle Carbon-13 NMR Study of CO_2 Adsorbed on Some Molecular Sieves. *J. Chem. Phys.* **1974**, *61* (6), 2351–2355.

[34] Omi, H.; Ueda, T.; Miyakubo, K.; Eguchi, T. Dynamics of CO_2 Molecules Confirmed in the Micropores of Solids as Studied by ^{13}C NMR. *Appl. Surf. Sci.* **2005**, *252* (3), 660–667.

[35] Čejka, J.; Van Bekkum, H.; Corma, A.; Schueth, F., *Introduction to Zeolite Molecular Sieves* volume 168, Elsevier, Amsterdam **2007**.

[36] Handy, N. C.; Cohen, A. J. Left-Right Correlation Energy. *Mol. Phys.* **2001**, *99* (5), 403–412.

[37] Lee, C. T.; Yang, W. T.; Parr, R. G. Development of the Colle-Salvetti Correlation-Energy Formula Into a Functional of the Electron Density. *Phys. Rev. B* **1988**, *37* (2), 785–789.

[38] Grimme, S.; Antony, J.; Ehrlich, S.; Krieg, H. A Consistent and Accurate *Ab Initio* Parametrization of Density Functional Dispersion Correction (DFT-D) for the 94 Elements H-Pu. *J. Chem. Phys.* **2010**, *132* (2), 154104.

[39] Grimme, S.; Ehrlich, S.; Goerigk, L. Effect of the Damping Function in Dispersion Corrected Density Functional Theory. *J. Comput. Chem.* **2011**, *32* (7), 1456–1465.

[40] Dunning, T. H. Gaussian Basis Sets for Use in Correlated Molecular Calculations. I. The Atoms Boron Through Neon and Hydrogen. *J. Chem. Phys.* **1989**, *90*, 1007–1023.

[41] Woon, D. E.; Dunning, T. H. Gaussian Basis Sets for Use in Correlated Molecular Calculations. III. The Atoms Aluminum Through Argon. *J. Chem. Phys.* **1993**, *98*, 1358–1371.

[42] Wolinski, K.; Hilton, J. F.; Pulay, P. Efficient Implementation of the Gauge-Independent Atomic Orbital Method for NMR Chemical Shift Calculations. *J. Am. Chem. Soc.* **1990**, *112*, 8251–8260.

[43] Kozuch, S.; Martin, J. M. L. DSD-PBEP86: In Search of the Best Double-Hybrid DFT with Spin-Component Scaled MP2 and Dispersion Corrections. *Phys. Chem. Chem. Phys.* **2011**, *13*, 20104–20107.

[44] Gauss, J. Calculation of NMR Chemical Shifts at Second-Order Many-Body Perturbation Theory Using Gauge-Including Atomic Orbitals. *Chem. Phys. Lett.* **1992**, *191* (6), 132–138.

[45] Stoychev, G. L.; Auer, A. A.; Neese, F. Efficient and Accurate Prediction of Nuclear Magnetic Resonance Shielding Tensors with Double-Hybrid Density Functional Theory. *J. Chem. Theory Comput.* **2018**, *14* (9), 4756–4771.

[46] Jensen, F. Segmented Constracted Basis Sets Optimized for Nuclear Magnetic Shielding. *J. Chem. Theory Comput.* **2015**, *11* (1), 132–138.

[47] Provasi, P. F.; Aucar, G. A.; Sauer, S. P. A. The Effect of Lone Pairs and Electronegativity on the Indirect Nuclear Spin−Spin Coupling Constants in CH_2X (X=CH_2, NH, O, S): *Ab Initio* Calculations Using Optimized Contracted Basis Sets. *J. Chem. Phys.* **2001**, *115* (3), 614–620.

[48] Kupka, T.; Stachów, M.; Nieradka, M.; Kaminsky, J.; Pluta, T. Convergence of Nuclear Magnetic Shieldings in the Kohn-Sham Limit for Several Small Molecules. *J. Chem. Theory Comput.* **2010**, *6*, 1580–1589.

[49] Montanari, T.; Busca, G. On the Mechanism of Adsorption and Separation of CO_2 on LTA Zeolites: An IR Investigation. *Vib. Spectrosc.* **2008**, *46* (1), 45–51.

[50] Galhotra, P.; Navea, J. G.; Larsen, S. C.; Grassian, V. H. Carbon Dioxide ($C^{16}O_2$ and $C^{18}O_2$)

Adsorption in Zeolite Y Materials: Effect of Cation, Adsorbed Water and Particle Size. *Energy Environ. Sci.* **2009**, *2* (4), 401–409.

[51] G. Busca, G.; Lorenzelli, V. Infrared Spectroscopic Identification of Species Arising from Reactive Adsorption of Carbon Oxides on Metal Oxide Surfaces. *Materials Chemistry* **1982**, *7* (1), 89–126.

[52] Huang, M.; Kaliaguine, S.; Auroux, A. Lewis Basic and Lewis Acidic Sites in Zeolites. *Stud. Surf. Sci. Catal.* **1995**, *97* (C), 311–318.

[53] Pirngruber, G. D.; Raybaud, P.; Belmabkhout, Y.; Čejka, J.; Zukal, A. The Role of the Extra-Framework Cations in the Adsorption of CO_2 on Faujasite Y. *Phys. Chem. Chem. Phys.* **2010**, *12* (41), 13534–13546.

[54] Busca, G. Bases and Basic Materials in Chemical and Environmental Processes. Liquid Versus Solid Basicity. *Chem. Rev.* **2010**, *110* (4), 2217–2249.

[55] Busca, G. Acidity and Basicity of Zeolites: A Fundamental Approach. *Microporous Mesoporous Mater.* **2017**, *254*, 3–16.